Supporting Information

Anisotropic Strain Tuning of $L1_0$ Ternary Nanoparticles for Oxygen Reduction

Junrui Li[1†‡], Shubham Sharma[2‡], Kecheng Wei[1], Zitao Chen[3,5], David Morris[4], Honghong Lin[1], Cheng Zeng[2], Miaofang Chi[3], Zhouyang Yin[1], Michelle Muzzio[1], Mengqi Shen[1], Peng Zhang[4], Andrew A. Peterson[2*], Shouheng Sun[1*]

[1]Department of Chemistry, Brown University, Providence, Rhode Island 02912, United States

[2]School of Engineering, Brown University, Providence, Rhode Island 02912, United States

[3]Center for Nanophase Materials Sciences Division, Oak Ridge National Laboratory, Oak Ridge, Tennessee 37831, United States

[4]Department of Chemistry, Dalhousie University, Halifax, Nova Scotia B3H 4R2, Canada

[5]The Wallace H. Coulter Department of Biomedical Engineering, Georgia Institute of Technology and Emory University, Atlanta, Georgia 30332, United States.

[†]Present address: Joint Center for Artificial Photosynthesis, Chemical Sciences Division, Lawrence Berkeley National Laboratory, Berkeley, California 94720, United States; Department of Materials Science and Engineering, University of California, Berkeley, California 94720, United States

[*]Corresponding Authors: Andrew A. Peterson: Andrew_Peterson@brown.edu. Shouheng Sun: ssun@brown.edu.

[‡]These authors contributed equally

Table S1. Reaction steps involved in dissociative mechanism (D_1-D_4) and associative mechanism (A_1-A_5).

Mechanism	***Reaction steps***
Dissociative mechanism	½ O_2 (g) + * → ½ *O_2 (D_1)
	½ *O_2 (g) + * → *O (D_2)
	*O + H^+ + e^- → *OH (D_3)
	*OH + H^+ + e^- → H_2O(l) + * (D_4)
Associative mechanism:	O_2 (g) + * → *O_2 (A_1)
	*O_2^* + H^+ + e^- → *OOH (A_2)
	*OOH + H^+ + e^- → H_2O(l) + *O (A_3)
	*O + H^+ + e^- → *OH (A_4)
	*OH + H^+ + e^- → H_2O(l) + * (A_5)

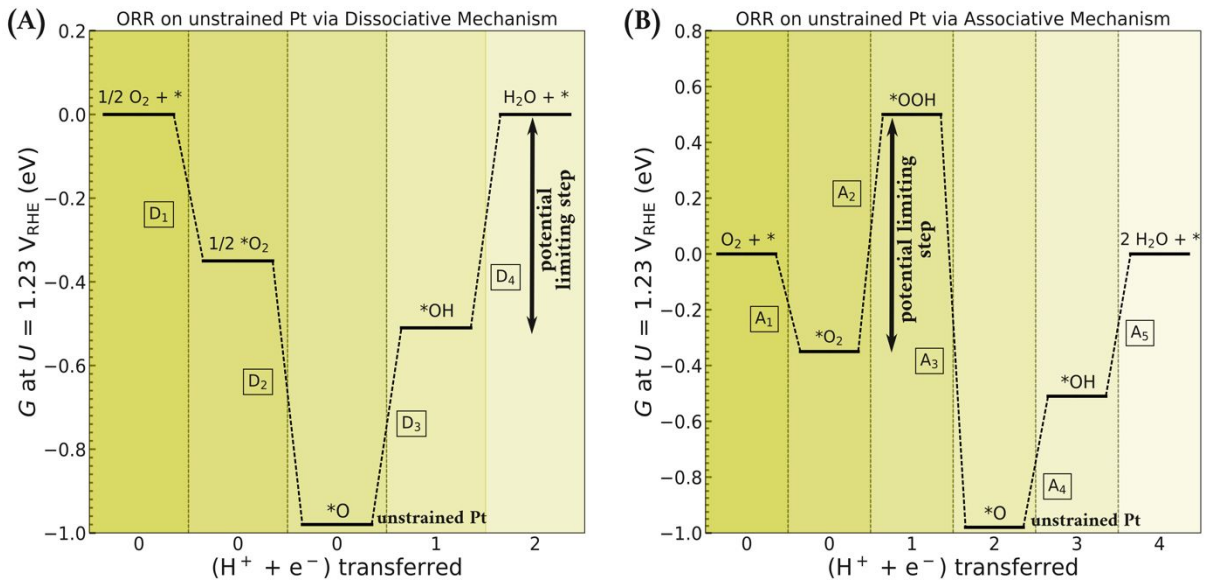

Figure S1. DFT-generated free energy landscapes at U = 1.23 V_{RHE} for ORR on unstrained Pt (111) surfaces via (A) dissociative and (B) associative mechanism.

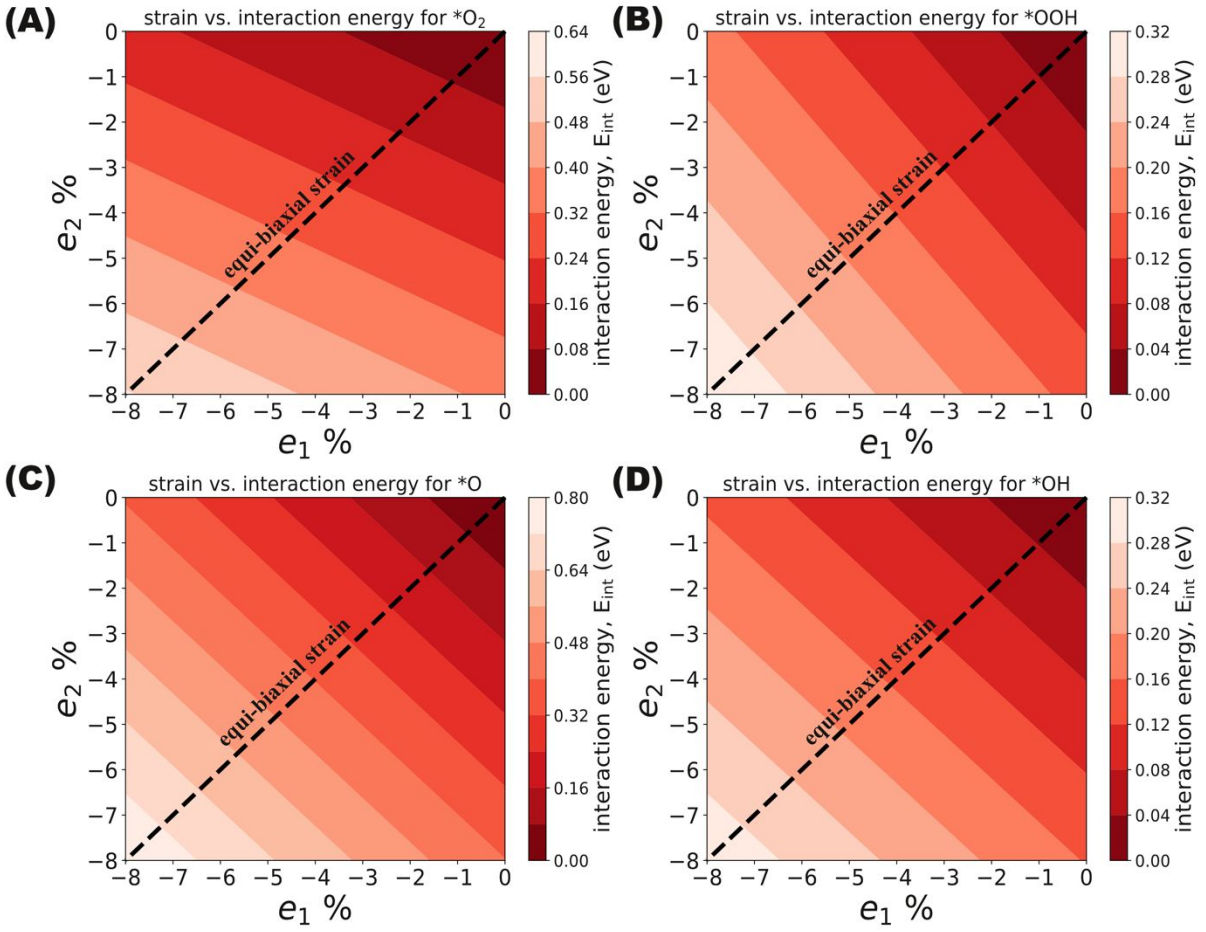

Figure S2. Eigenforce model-generated interaction energies as a function of 2D strain for (**A**) *O_2, (**B**) *OOH, (**C**) *O and (**D**) *OH.

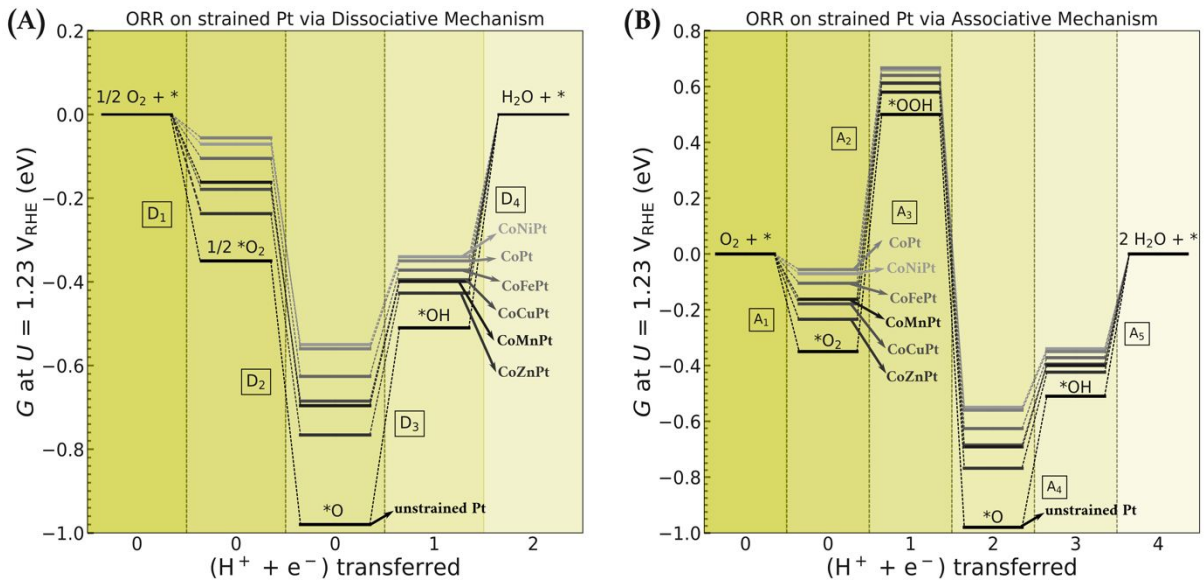

Figure S3. Computationally generated free energy landscapes at U = 1.23 V_{RHE} for ORR on $L1_0$-strained and unstrained Pt (111) surfaces via (**A**) dissociative and (**B**) associative mechanisms. The unstrained Pt surface data was generated using DFT calculations, while the eigenforce model was used for $L1_0$-strained Pt surfaces.

Table S2. Calculated change in free energies for the steps involved in the dissociative mechanism on strained $L1_0$ and unstrained fcc Pt (111) surfaces. Note that the values obtained for unstrained Pt are through DFT calculations while the eigenforce model was used for the strained surfaces. The step highlighted in bold denotes the potential-limiting step.

System	D_1 (eV)	D_2 (eV)	D_3 (eV)	D_4 (eV)
Unstrained Pt	-0.350	-0.630	0.470	**0.510**
$L1_0$-CoNiPt	-0.071	-0.484	0.21	**0.342**
$L1_0$-CoPt	-0.056	-0.503	0.213	**0.349**
$L1_0$-CoFePt	-0.105	-0.520	0.254	**0.372**
$L1_0$-CoCuPt	-0.179	-0.505	0.289	**0.395**
$L1_0$-CoMnPt	-0.162	-0.533	0.296	**0.399**
$L1_0$-CoZnPt	-0.237	-0.529	0.339	**0.427**

Table S3. Calculated change in free energies for the steps involved in the associative mechanism on strained $L1_0$ and unstrained fcc Pt (111) surfaces. Note that the values obtained for unstrained Pt are through DFT calculations while the eigenforce model was used for the strained surfaces. The step highlighted in bold denotes the potential-limiting step.

System	A_1 (eV)	A_2 (eV)	A_3 (eV)	A_4 (eV)	A_5 (eV)
Unstrained Pt	-0.350	**0.850**	-1.480	0.470	0.510
$L1_0$-CoNiPt	-0.071	**0.737**	-1.221	0.21	0.342
$L1_0$-CoPt	-0.056	**0.723**	-1.226	0.213	0.349
$L1_0$-CoFePt	-0.105	**0.746**	-1.266	0.254	0.372
$L1_0$-CoCuPt	-0.179	**0.792**	-1.297	0.289	0.395
$L1_0$-CoMnPt	-0.162	**0.774**	-1.307	0.296	0.399
$L1_0$-CoZnPt	-0.237	**0.817**	-1.346	0.339	0.427

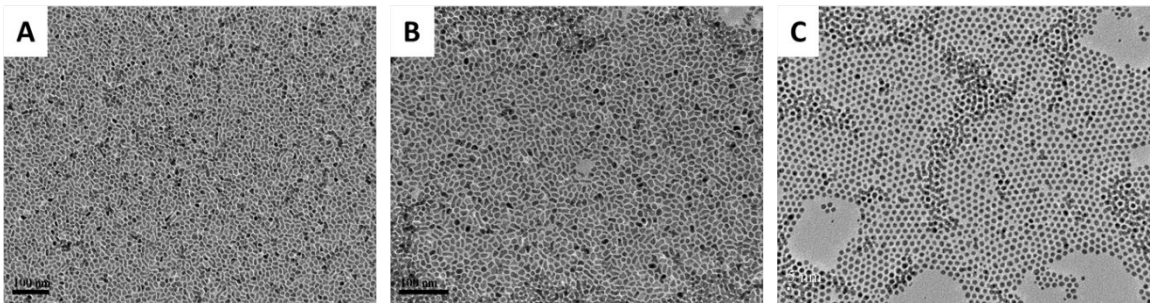

Figure S4. TEM images of as-synthesized (A) $Co_1Ni_2Pt_3$, (B) $Co_2Ni_1Pt_3$ and (C) Ni_1Pt_1 NPs.

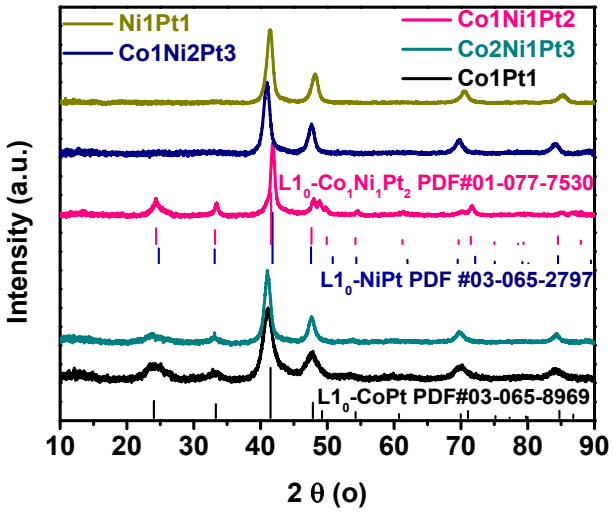

Figure S5. XRD patterns of Ni_1Pt_1, $Co_1Ni_2Pt_3$, $Co_1Ni_1Pt_2$, $Co_2Ni_1Pt_3$ and Co_1Pt_1 NPs annealed under 95 % Ar + 5% H_2 at 650 ^oC for 6 h.

Table S4. Composition ratio and Pt loading of C-loaded $L1_0$-NPs after post-acid treatment and annealing calculated from ICP results.

Sample	*composition*	*Pt loading (mg)*
$L1_0$-CoPt	$Co_{48}Pt_{52}$	11.7
$L1_0$-CoMnPt	$Co_{28}Mn_{20}Pt_{52}$	10.8
$L1_0$-CoFePt	$Co_{25}Fe_{30}Pt_{45}$	14.4
$L1_0$-CoNiPt	$Co_{29}Ni_{25}Pt_{46}$	12.6
$L1_0$-CoCuPt	$Co_{25}Cu_{27}Pt_{47}$	10.8
$L1_0$-CoZnPt	$Co_{19}Zn_{20}Pt_{61}$	12.1

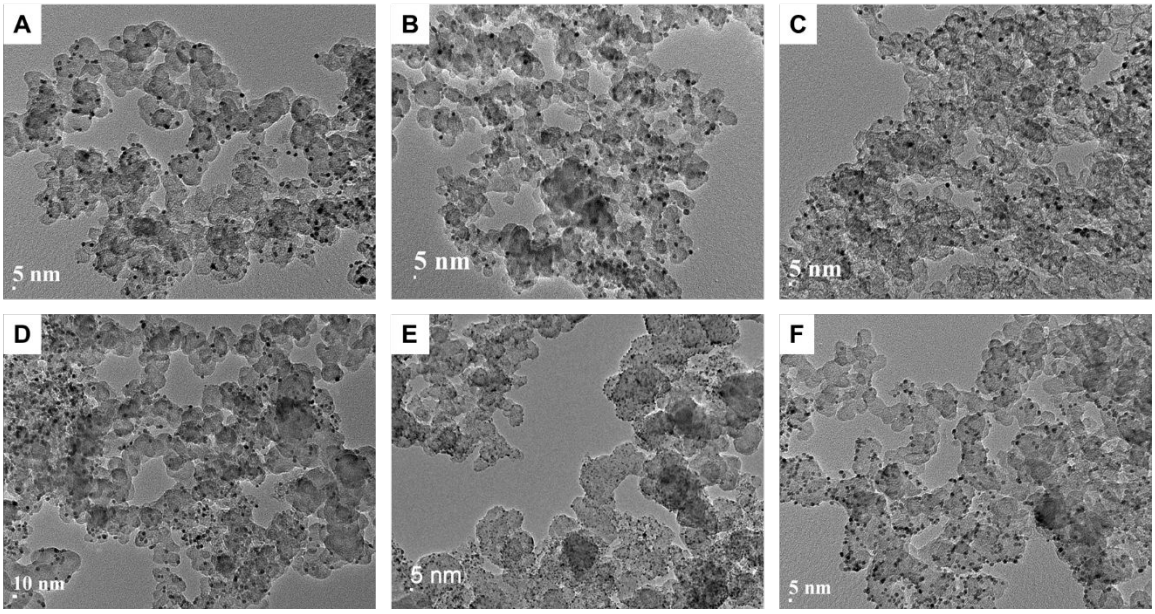

Figure S6. TEM images of C-loaded (A) $L1_0$-CoPt NPs, (B) $L1_0$-CoMnPt NPs, (C) $L1_0$-CoFePt NPs, (D) $L1_0$-CoNiPt NPs, (E) $L1_0$-CoCuPt and (F) $L1_0$-CoZnPt NPs after annealing treatment.

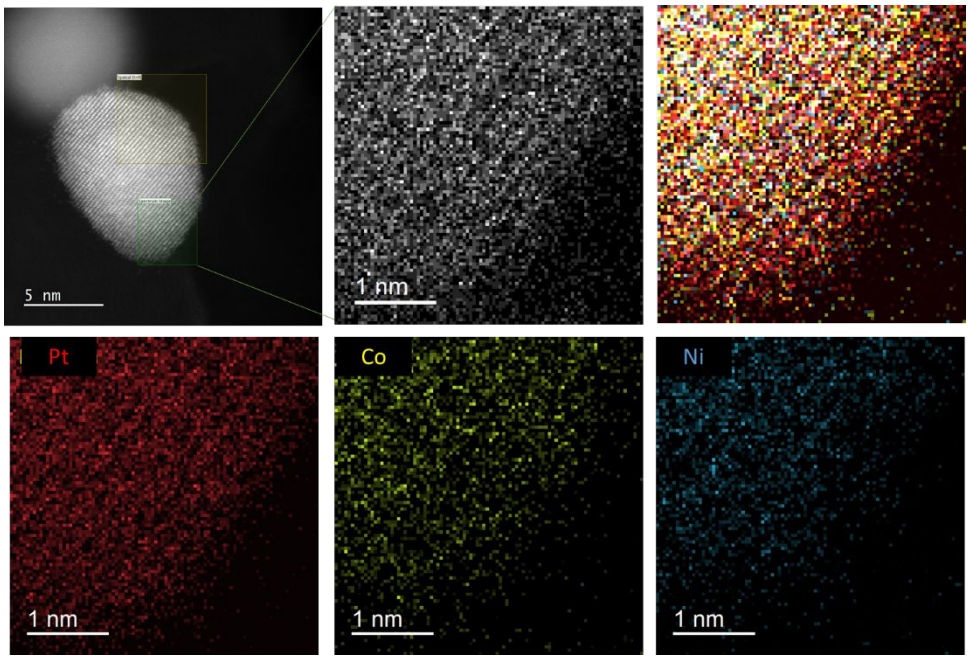

Figure S7. Atomic resolution elemental mapping images showing the alternative layers of Pt and Co/Ni.

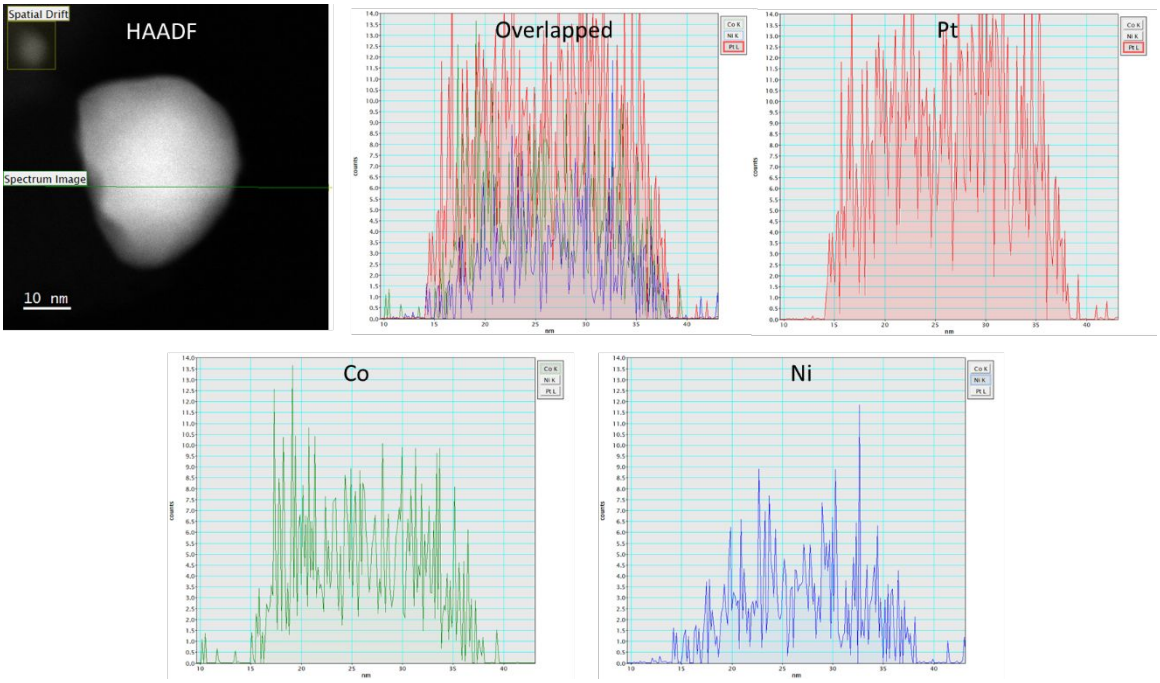

Figure S8. A HAADF image and a line-scan profile showing the distribution of Pt, Co and Ni components in core/shell structured $L1_0$-CoNiPt NPs.

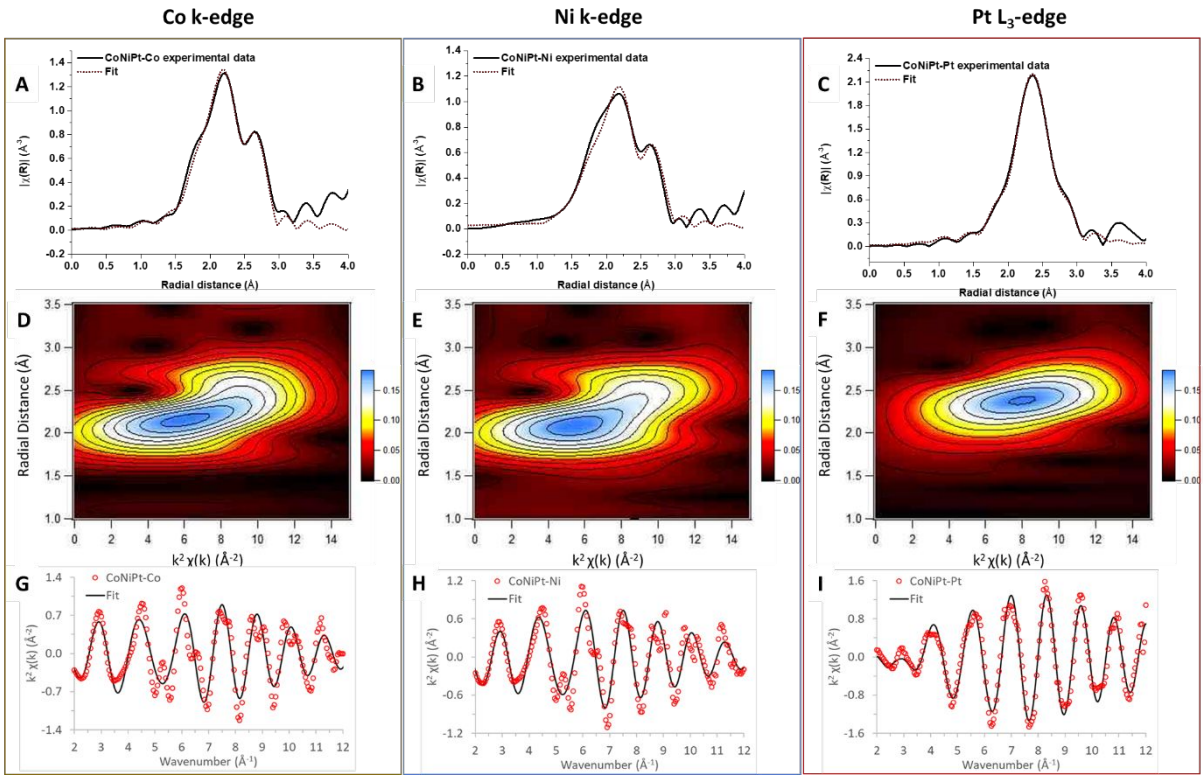

Figure S9. EXAFS experimental data and fitting results of Co K-edge, Ni K-edge and Pt L_3-edge. (A)-(C) FT-EXAFS spectra and best fit. (D)-(F) Contour map of k-space data. (G)-(I) k-space data and best fit.

Table S5 Fitting parameters, including coordination number (CN) and bond length (R), obtained from the fitting results of Pt L_3-edge EXAFS data.

bond	*CN*	*R (Å)*	*σ^2 (Å) x10^{-3}*	*E_0 (eV)*	*R factor*
Pt-Pt	6(2)	2.69(1)	4(2)	6(1)	0.0138
Pt-Co/Ni	5(2)	2.652(6)	6(3)	6(1)	0.0138

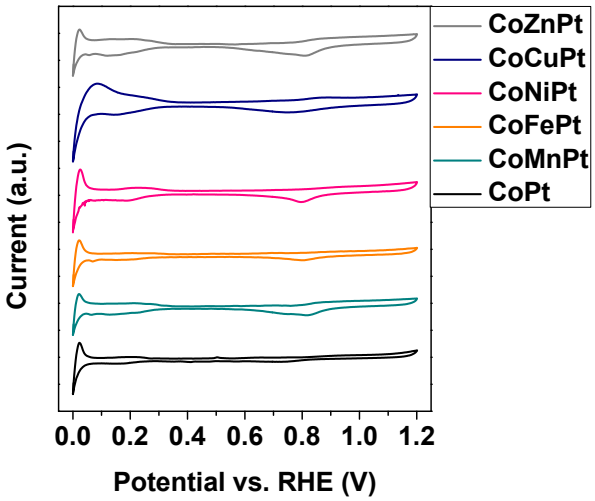

Figure S10. Cyclic voltammetry curves of C-$L1_0$-CoMPt NPs obtained in N_2-saturated 0.1 M $HClO_4$ at room temperature.

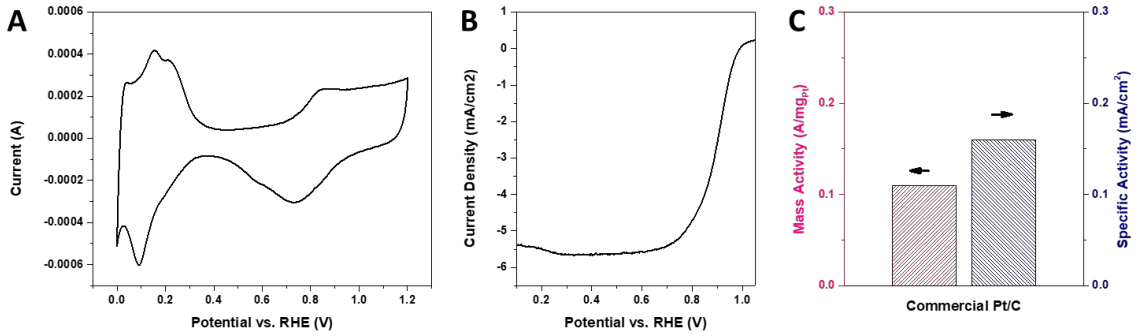

Figure S11. (**A**) Cyclic voltammetry curve of commercial Pt/C obtained in N_2-saturated 0.1 M $HClO_4$ at room temperature. (**B**) Linear scanning voltammetry curve of commercial Pt/C collected in O_2-saturated 0.1 M $HClO_4$ at room temperature. (**C**) Mass activity and specific activity calculated on commercial Pt/C.

Table S6. DFT optimized lattice constants using RPBE exchange-correlation functional.

System	a (Å)	b (Å)	C (Å)
Unstrained Pt	3.99	3.99	3.99
$L1_0$-CoZnPt	3.97	3.97	3.70
$L1_0$-CoMnPt	3.90	3.90	3.80
$L1_0$-CoCuPt	3.94	3.94	3.66
$L1_0$-CoFePt	3.86	3.86	3.82
$L1_0$-CoPt	3.83	3.83	3.78
$L1_0$-CoNiPt	3.87	3.87	3.69